Maximum Thrust Nozzles for Nonequilibrium Simple Dissociating Gas Flows

M. Peter Scofield* and Joe D. Hoffman†
Purdue University, Lafayette, Ind.

A formulation, numerical solution technique, and computer program implementing the technique are presented for the design of maximum thrust nozzles for rotational or nonequilibrium simple dissociating gas flows including boundary-layer effects. The formulation is based on the usual assumptions applicable to rotational and nonequilibrium simple dissociating gas flows and on the assumption that the boundary layer is thin. The thrust is maximized by application of the calculus of variations. The resulting design equations are hyperbolic partial differential equations, which are solved by the method of characteristics. The results of a study to determine the magnitude of the performance increases that can be expected by considering more accurate flow chemistry models are presented. The results indicate that significant performance improvements may be possible.

Nomenclature

a = acoustic speed
C,C_e = nonequilibrium and equilibrium atomic mass fraction, respectively, of simple dissociating gas
C_i = mass fraction of general species i
C_p,C_{pi} = constant pressure specific heat of mixture and species i, respectively
d = width of two-dimensional nozzle
f = thrust function, Eq. (19)
g = generalized isoperimetric constraint, Eq. (12)
h,h_i = enthalpy of mixture and species i, respectively
k_r = reverse reaction rate constant
p,p_0 = pressure and ambient pressure, respectively
R,R_2 = gas constant of mixture and molecule, respectively
T = temperature
u,v = axial and radial velocity component, respectively
V = velocity modulus, $V = (u^2 + v^2)^{1/2}$
W_2 = molecular weight of molecular species
x,y = axial and radial spacial coordinate, respectively
α = Mach angle, $\alpha = \sin^{-1}(1/M)$
β_i = Lagrange multipliers, $i = 1,2$
γ = specific heat ratio
δ = $\delta^* \cos\theta$
δ^* = boundary-layer displacement thickness
η,η_w = inviscid core boundary and nozzle wall, respectively
θ = flow angle, $\theta = \tan^{-1}(v/u)$
λ_i = Lagrange multipliers ($i = 1,2,3,4,5$)
ν = 0, two-dimensional flow; 1, axisymmetric flow
ρ = density
σ = atomic species source function, Eq. (10)
τ = wall shear stress
ψ = thermodynamic function, Eq. (9)

Subscripts and Superscripts

F = evaluated at wall point F
$C,p,T,$ $u,v,x,$ $\eta,\dot{\eta}$ = partial derivative with respect to that variable
$(\dot{})$ = total differentiation with respect to x

Presented as Paper 70-707 at the AIAA 6th Propulsion Joint Specialist Conference, San Diego, Calif., June 15–19, 1970; received July 10, 1970; revision received December 7, 1970. This investigation was sponsored by the Air Force Aero Propulsion Laboratory, Wright-Patterson Air Force Base, Ohio, under Contract F33615-67-C-1068.

* Research Assistant in Mechanical Engineering. Associate Member AIAA.

† Associate Professor of Mechanical Engineering. Member AIAA.

Introduction

A SIGNIFICANT difference generally exists between the actual performance and the predicted isentropic performance of many jet propulsion engines. A large part of the performance loss occurs in the exhaust expansion system as a result of nonequilibrium chemical reactions, gradients in stagnation conditions and mixture ratio, and boundary-layer effects. In the scramjet engine, where losses in gross thrust can be magnified several times in net thrust, the degradation of engine performance can be so severe that the effectiveness of the engine could be impaired. In view of the serious effects these nonideal processes can have on the performance of both air-breathing and rocket engines, it is imperative that they be given very careful consideration in the design of the expansion nozzle for such engines.

The present analysis presents the formulation of an optimization technique, a numerical solution method, and a computer program for the design of two-dimensional and axisymmetric thrust nozzles when the working fluid is either a simple dissociating gas in chemical nonequilibrium or a general gas mixture whose composition is either frozen or in chemical equilibrium. The effects of the boundary-layer thickness and the wall shear stress are included in the formulation and computer program.

The first application of sophisticated optimization techniques to the design of thrust nozzles was made by Guderley and Hantsch,[1] who considered the problem of irrotational flow (isentropic throughout) through an axisymmetric nozzle of fixed length. Later, this same problem was considered by Rao,[2] who developed a formulation and solution technique that has proved much easier to apply. Currently, Rao's technique is in wide use throughout the propulsion industry. The differences between the formulations of Ref. 1 and Ref. 2 were analyzed by Guderley,[3] who extended the development to include isentropic flows with entropy variations between streamlines. These three formulations were all developed along the one-dimensional control surface, illustrated in Fig. 1, consisting of the left-running Mach line CKF. Since the path taken by streamlines was not considered in the development, the formulations are valid only for flows in which no dissipative effects occur.

The problem of obtaining the optimum nozzle contour for a general geometrical constraint was formulated by Guderley

and Armitage.[4] Although their formulation was restricted to nondissipative flows, it can be extended to include flows with dissipative processes since the entire flowfield in the region IKFI, Fig. 1, is considered in the formulation. The formulation presented in this work is based on this general approach.

The problem of minimizing the recombination losses in a one-dimensional nozzle was investigated by Appleton[5]; however, two-dimensional effects and exit divergence losses were not considered. A nozzle design technique for two-dimensional, nonequilibrium flows based on truncated perfect nozzles was developed by Burwell, Sarli and Zupnik.[6] Although the truncated perfect nozzle is not an optimum nozzle, the results obtained by such an approach can be useful. Kraiko et al.[7,8] developed the design equations for minimum wave drag bodies and maximum thrust nozzles for both irrotational and nonequilibrium flows. Various body shapes, some of which included base pressure effects, were investigated. A one-dimensional formulation and numerical solution for the maximum thrust problem for nonequilibrium flow including annular base pressure effects was developed by Galyun and Kraiko.[9] However, divergence and boundary-layer effects were not considered. Hoffman[10] developed a general nozzle design technique for two-dimensional and axisymmetric flow of a general gas mixture in chemical nonequilibrium. Scofield, Thompson, and Hoffman[11] developed a design technique and computer program for the design of maximum thrust nozzle contours including boundary-layer effects for irrotational flowfields. The formulations of Refs. 10 and 11 were combined and extended by Hoffman, Scofield, and Thompson[12] to include a general gas mixture in chemical nonequilibrium, a simple dissociating gas in chemical nonequilibrium, and a general gas mixture whose composition is either frozen or in chemical equilibrium, all including boundary-layer effects.

The formulation presented in this work is developed in Ref. 13. A numerical relaxation procedure is presented for applying the resulting design equations. A sample case is presented to demonstrate the technique. A brief parametric study is presented to illustrate the magnitude of the performance improvement which can be obtained. This procedure represents a significant advancement in the numerical solution of the general two-dimensional nozzle design problem.

Analysis

Introduction

There are two basic approaches to thrust nozzle optimization. The first and more simple approach poses the extremal problem of maximizing the thrust written in terms of the flow variables along a control surface passing through the nozzle exit lip. In this approach, the only constraints that can be imposed are those directly expressible in terms of this control surface. Thus, constraints such as constant wall arc length or nozzle surface area can not be imposed on the problem. In addition, flows with dissipative effects can not be considered since the flow properties at the control surface depend on the path of each streamline. Because the control surface reduces to a line for two-dimensional or axisymmetric flows, the variational problem becomes one-dimensional. In general, one-dimensional problems are more easily solved than those in two or three dimensions.

The second basic approach, and the one employed in the current work, poses the extremal problem of maximizing the thrust written in terms of the forces acting on the nozzle wall. In this approach, the entire region IKFI in Fig. 1 is considered, and as a result, flows with dissipative effects such as finite rate chemistry or particle drag and heat transfer can be included. Boundary-layer effects and a general geometrical constraint may also be included in the formulation. Because of the resultant two-dimensional nature and increased generality of this approach, the solution becomes much more complex. However, with high-speed computers the numerical solution of such problems is feasible.

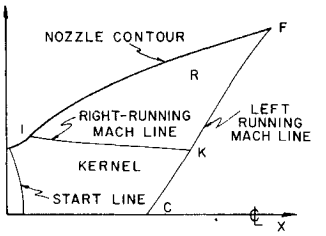

Fig. 1 Nozzle geometry and flowfield model.

Gas Dynamic Model

Two gas dynamic models are considered in this study. The first is a simple dissociating gas (i.e., a homonuclear, diatomic gas) in chemical nonequilibrium. The governing reaction is the dissociation-recombination reaction between the atoms and the molecule in the presence of a third body, which consists of the other atoms and molecules of the gas. The individual species are assumed to be thermally perfect gases. The second is a general gas mixture of any number and type of species whose composition is fixed (i.e., frozen) or determined from equilibrium thermodynamics (i.e., equilibrium). In both cases, variations in stagnation pressure and enthalpy are allowed across the flowfield, resulting in a rotational flow.

The governing equations for the steady flow of a simple dissociating gas in the absence of transport phenomena and body forces are as follows (see Ref. 13):

$$y^\nu \rho u_x + y^\nu \rho v_y + y^\nu u \rho_x + y^\nu v \rho_y + \nu \rho v = 0 \tag{1}$$

$$\rho u u_x + \rho v u_y + p_x = 0 \tag{2}$$

$$\rho u v_x + \rho v v_y + p_y = 0 \tag{3}$$

$$u p_x + v p_y - a^2 u \rho_x - a^2 v \rho_y + \psi = 0 \tag{4}$$

$$\rho u C_x + \rho v C_y - \sigma = 0 \tag{5}$$

$$p = \rho T R_2 (1 + C) \tag{6}$$

$$h = \sum_{i=1}^{2} h_i C_i \tag{7}$$

$$h_i = h_{i0} + \int_{T_0}^{T} C_{pi} dT \quad (i = 1,2) \tag{8}$$

$$\psi = [(\gamma - 1)(h_1 - h_2) - \gamma R_2 T]\sigma \tag{9}$$

$$\sigma = 4\rho^2 k_r (1 + C)(C_e^2 - C^2)/W_2^2 (1 - C_e^2) \tag{10}$$

A general gas mixture, when frozen or in equilibrium, obeys Eqs. (1–4) with $\psi = 0$. Thus, both gas models can be considered simultaneously in the optimization formulation, and the results for the general mixture can be obtained by setting $\psi = 0$ and dropping Eq. (5). In addition, the general gas mixture requires relationships between V, p, T, and a along streamlines. Such relationships can be expressed in tabular form, and need not be restricted to thermally perfect gases.

Boundary-Layer Model

Boundary-layer effects are considered in the formulation by including the wall shear stress τ and an integral boundary-layer thickness δ^* in the expression for the thrust integral. To retain generality, no particular expressions for τ and δ^* are assumed; however, they are restricted to be functions only of the radial coordinate y. This restriction is necessary to decouple the interaction of the boundary layer and the flowfield in the variational problem. The interaction must be one-way (flowfield on boundary layer and not vice versa) in order to preserve the tack-on nature of the boundary-layer

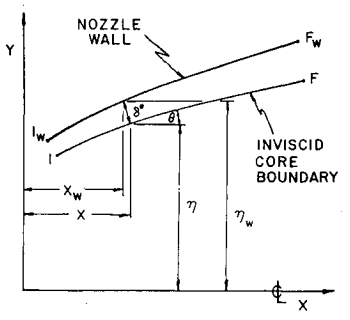

Fig. 2 Model for thrust evaluation.

model. The thickness δ^* is normally taken to be the displacement thickness, although this is not required in the general analysis.

Formulation of the Design Problem

The extremal problem is formulated by considering the thrust produced by the supersonic portion of the nozzle flowfield, which is obtained by integrating the axial components of the pressure force and the shear drag acting on the nozzle wall. If x_I and x_F are the axial coordinates of the end points of the wall, then the thrust generated is given by the following equation (see Fig. 2):

$$\frac{\text{THRUST}}{2\pi^{\nu}\text{d}^{(1-\nu)}} = \int_{x_I}^{x_F} [(p - p_0)(\dot{\eta} + \dot{\delta}) - \tau](\eta + \delta)^{\nu} dx \quad (11)$$

where $y = \eta(x)$ is the inviscid core boundary to be determined from the analysis.

From Fig. 1, it can be seen that if the lines IK and KF are right- and left-running Mach lines respectively, only the portion of the flowfield enclosed in the region IKFI will be affected by changes in the nozzle wall contour between points I and F. Hence, only the region IKFI is considered in the formulation of the optimization problem. The condition that the boundary KF is a left-running Mach line is obtained later from the analysis. Thus, the contour obtained is optimum only for the arbitrarily specified upstream geometry. The effect of the upstream geometry can be studied parametrically to determine the best combination of upstream geometry and supersonic contour.

The gas dynamic flow model is introduced into the variational problem by employing the flowfield governing equations, Eqs. (1–5), as constraints which will apply throughout the entire region IKFI. This is accomplished by multiplying each by a Lagrange multiplier, integrating over region IKFI, and adding the result to the thrust equation.

The geometrical or engineering restriction is imposed on the nozzle contour by a general isoperimetric constraint, that is, one in which the integral of some function along the boundary must be constant. Thus, the expression

$$\int_{x_I}^{x_F} g(x,\eta,\dot{\eta},p)dx = \text{const} \quad (12)$$

is multiplied by a constant Lagrange multiplier and added to the thrust equation. If $g = 1$, a constant length nozzle is specified. Examples of other constraints are presented in Ref. 13.

The formulation of the problem is completed by specifying that the inviscid core boundary IF be a streamline. This is accomplished by multiplying the equation of a streamline by a Lagrange multiplier, integrating along IF, and adding the result to the thrust equation. Thus

$$\eta^{\nu}\rho(u\dot{\eta} - v) = 0 \quad \text{on IF} \quad (13)$$

The term $\eta^{\nu}\rho$ is included to simplify future operations.

The following functional, which is to be maximized, is obtained when all of the above constraints are added to the thrust equation

$$I = \int_R F dxdy + \int_{\text{IKFI}} G dx \quad (14)$$

where

$$F = \lambda_1(y^{\nu}\rho u_x + y^{\nu}\rho v_y + y^{\nu}u\rho_x + y^{\nu}v\rho_y + \nu\rho v) + \lambda_2(\rho u u_x + \rho v u_y + p_x) + \lambda_3(\rho u v_x + \rho v v_y + p_y) + \lambda_4(up_x + vp_y - a^2u\rho_x - a^2v\rho_y + \psi) + \lambda_5(\rho u C_x + \rho v C_y - \sigma) \quad \text{in } R \quad (15)$$

$$G = 0 \quad \text{on IK and KF} \quad (16)$$

$$G = -[f + \beta_1\eta^{\nu}\rho(u\dot{\eta} - v) + \beta_2 g] \quad \text{on FI} \quad (17)$$

$$f = [(p - p_0)(\dot{\eta} + \dot{\delta}) - \tau](\eta + \delta)^{\nu} \quad (18)$$

The Lagrange multipliers λ_1–λ_5 are functions of x and y, β_1 is a function of x, and β_2 is a constant. The gas dynamic properties u, v, p, ρ, and C are functions of x and y.

The fundamental function F is the only portion of the functional to be maximized that includes the gas dynamic model. The fundamental function defined by Eq. (15) is for the simple dissociating gas model. For the frozen or equilibrium flow (rotational) model, the fundamental function is given by Eq. (15) with $\psi = \lambda_5 = 0$. The functions G and f are the same for the two gas models. Thus, all future derivations and results are for the simple dissociating gas model, and results valid for the rotational flow model can be obtained by simply discarding those terms which contain the chemical kinetics effects (namely, terms containing ψ, C or λ_5, their partial derivatives, or partial derivatives with respect to C).

With the complete functional formed, the problem now is to find that special function $y = \eta(x)$ which, subject to prescribed initial conditions and constraints, maximizes I of Eq. (14).

Necessary Conditions

In the calculus of variations, three general conditions must be satisfied if an extremal of a function is to be found. These are the Euler equations, the transversality conditions, and the corner conditions.

The Euler equations are partial differential equations which determine the Lagrange multipliers in region IKFI. These equations arise when the coefficients of the variations of the dependent variables resulting from the first variation of the fundamental function are set to zero. The Euler equations, derived in Ref. 13, are as follows:

$$y^{\nu}\lambda_{1x} + u\lambda_{2x} + v\lambda_{2y} - \lambda_2 u_x - \lambda_3 v_x - (\lambda_4/\rho)(p_x - a^2\rho_x) - \lambda_5 C_x = \lambda_2(\nu v/y) \quad (19)$$

$$y^{\nu}\lambda_{1y} + u\lambda_{3x} + v\lambda_{3y} - \lambda_2 u_y - \lambda_3 v_y - (\lambda_4/\rho)(p_y - a^2\rho_y) - \lambda_5 C_y = \lambda_3(\nu v/y) \quad (20)$$

$$\lambda_{2x} + \lambda_{3y} + u\lambda_{4x} + v\lambda_{4y} + \lambda_4(u_x + v_y) + \lambda_4 a_p{}^2(u\rho_x + v\rho_y) = \lambda_4\psi_p - \lambda_5\sigma_p \quad (21)$$

$$-y^{\nu}(u\lambda_{1x} + v\lambda_{1y}) + a^2(u\lambda_{4x} + v\lambda_{4y}) + \lambda_4 a^2(u_x + y_y) + (\lambda_4 a_p{}^2 u - \lambda_2/\rho)p_x + (\lambda_4 a_p{}^2 v - \lambda_3/\rho)p_y = -\lambda_4\psi_\rho + \lambda_5\sigma_\rho - (\lambda_4 a_C{}^2 + \lambda_5)\sigma/\rho \quad (22)$$

$$\rho u\lambda_{5x} + \rho v\lambda_{5y} + \lambda_4 a_C{}^2(u\rho_x + v\rho_y) = \lambda_5(\nu\rho v/y) + \lambda_4\psi_C - \lambda_5\sigma_C \quad (23)$$

The symbols $a_p{}^2$ and $a_C{}^2$ denote the partial derivatives of the sound speed squared with respect to p and C.

In order to determine the Lagrange multipliers, boundary conditions are required. These are obtained from the transversality and corner conditions. The transversality conditions arise when the dependent variables on the boundary

or the boundary itself are allowed to vary. The corner condition must be included when corner points exist on the boundary. For the current formulation, the following variations on the region boundary are allowed. The boundary line IK is assumed to be specified; therefore, the contour obtained is optimum only for the a priori specified upstream flowfield. The boundary lines KF and FI are allowed to be completely free. The corner points I and K are fixed. The corner point F is completely free. The boundary conditions for the Lagrange multipliers resulting from the transversality and corner conditions are presented in the next section. The derivations of these conditions are presented in Ref. 13.

Summary of Resulting Equations

The flow field governing equations, Eqs. (1–5), and the Euler equations, Eqs. (19–23), yield ten partial differential equations for determining the ten variables $u, v, p, \rho, C, \lambda_1, \lambda_2, \lambda_3, \lambda_4$, and λ_5. These equations form a system of first-order, quasi-linear, nonhomogeneous, partial differential equations of the hyperbolic type when the flow is supersonic. Therefore, this system of equations can be replaced by an equivalent system of characteristic and compatibility equations, which are first-order, ordinary differential equations valid along the characteristic lines, which are streamlines and Mach lines. The following system of equations is obtained. Along streamlines

$$dy/dx = v/u \tag{24}$$

$$\rho u du + \rho v dv + dp = 0 \tag{25}$$

$$u dp - a^2 u d\rho = -\psi dx \tag{26}$$

$$\rho u dC = \sigma dx \tag{27}$$

$$-y^\nu d\lambda_1 + a^2 d\lambda_4 + \lambda_2 du + \lambda_3 dv + (\lambda_4/\rho)(\rho a_p{}^2 - 1)dp = \{(\lambda_4 a^2/u)vv/y - [\lambda_4\psi_\rho - \lambda_5\sigma_\rho + (\lambda_4 a_C{}^2 + \lambda_5)\sigma/\rho]/u + \lambda_4\psi/\rho u\}dx \tag{28}$$

$$y^\nu d\lambda_1 + u d\lambda_2 + v d\lambda_3 - \lambda_2 du - \lambda_3 dv = [(vv/y)(\lambda_2 + \lambda_3 v/u) - (\lambda_4\psi - \lambda_5\sigma)/\rho u]dx \tag{29}$$

$$\rho u d\lambda_5 + \lambda_4 a_C{}^2 u d\rho = (\nu\lambda_5\rho v/y + \lambda_4\psi_C - \lambda_5\sigma_C)dx \tag{30}$$

Along Mach lines

$$dy/dx = \tan(\theta \pm \alpha) \tag{31}$$

$$\pm \cot\alpha dp/\rho + u dv - v du = (v - u dy/dx)(vv/y + \psi/\rho a^2)dx \tag{32}$$

$$-y^\nu d\lambda_1 \pm \tan\alpha(v d\lambda_2 - u d\lambda_3) + \lambda_2 du + \lambda_3 dv + \lambda_5 dC + \lambda_4(dp - a^2 d\rho)/\rho = \pm(vv/y)\tan\alpha(\lambda_2 dy/dx - \lambda_3)dx + \tan\alpha\{\lambda_4[(\rho a_p{}^2 - 1)\psi/\rho - a^2\psi_p - \psi_\rho - a_C{}^2\sigma/\rho] + \lambda_5(a^2\sigma_p + \sigma_\rho)\}\frac{dx}{a\cos(\theta \pm \alpha)} \tag{33}$$

The upper signs refer to left Mach lines and the lower signs to right Mach lines. The partial derivatives of σ, ψ, and a^2 appearing in the above equations are presented in Ref. 13.

The boundary conditions for the Lagrange multipliers along FI are given by the following expressions:

$$\beta_1 = \lambda_1 \tag{34}$$

$$\lambda_3 = \lambda_2\dot{\eta} - f_p - \beta_2 g_p \tag{35}$$

$$\lambda_1 = \lambda_{1_F} + \int_x^{x_F} (1/\eta^\nu)[f_p dv/dx - (f_\eta - df_{\dot{\eta}}/dx)/\rho u]dx + \beta_2 \int_x^{x_F} (1/\eta^\nu)[g_p dv/dx - (g_\eta - dg_{\dot{\eta}}/dx)/\rho u]dx \tag{36}$$

$$\lambda_{1_F} = -(1/\eta^\nu \rho u)(f_{\dot{\eta}} + \beta_2 g_{\dot{\eta}})|_F \tag{37}$$

$$\beta_2 = -f/g|_F \tag{38}$$

The boundary conditions along KF are:

$$\lambda_1 y^\nu \dot{y} + \lambda_2(u\dot{y} - v) = 0 \tag{39}$$

$$\lambda_1 y^\nu - \lambda_3(u\dot{y} - v) = 0 \tag{40}$$

$$\lambda_1 y^\nu - \lambda_4 a^2 = 0 \tag{41}$$

$$\lambda_5 = 0 \tag{42}$$

Method of Solution

An examination of the resulting equations shows that, once the nozzle flowfield has been determined, there are a sufficient number of equations and boundary conditions to determine the Lagrange multipliers. Actually, there is one extra boundary condition; it is this extra boundary condition that serves as a check to determine whether or not an assumed nozzle contour is an optimum contour. Thus, the solution procedure for the determination of an optimum nozzle contour is an iterative procedure. That is, an initial wall contour is assumed, and the flow and Lagrange multiplier fields are calculated. Then the extra boundary condition is checked, and if this extra condition is satisfied, the assumed contour is optimum. If it is not, then the nozzle wall must be adjusted by a relaxation technique, and the above process repeated until the check condition is satisfied.

The Lagrange multipliers are determined in the following manner. First the flowfield is calculated for some assumed contour, and the multipliers at point F are evaluated using Eqs. (37) and (38). Then all the multipliers along the exit Mach line KF starting at point F are determined by the simultaneous solution of Eq. (33) for the left-running Mach line with Eqs. (39–42). Using these values along KF and Eqs. (28–30) and (33), the multiplier field is calculated throughout the region IKFI. The procedure is initiated at point F and continued down to IK. When the solution along the boundary FI is sought, Eq. (36) is used to evaluate λ_1, and the left-running Mach line compatibility equation of Eq. (33) is omitted.

In order to determine if the assumed contour is optimum, Eq. (35), which was not used in the above scheme, is evaluated using the known multipliers and flow variables along FI. If Eq. (35) is indeed satisfied, the assumed contour is an optimum contour; if it is not, then the wall contour must be adjusted until Eq. (35) is satisfied. A relaxation technique for adjusting the nozzle contour is presented in the following section.

Relaxation Technique

A relaxation technique for adjusting the nozzle wall is obtained by rewriting Eq. (35) in terms of an error function E.

$$E = \lambda_3 - \dot{\eta}\lambda_2 + f_p + \beta_2 g_p \tag{43}$$

When expanded, using the particular form of f_p obtained from Eq. (18) and considering constraints which do not depend on p so $g_p = 0$, E becomes

$$E = \lambda_3 - \dot{\eta}\lambda_2 + (1 + d\delta/d\eta)(\eta + \delta)^\nu\dot{\eta} \tag{44}$$

Generally, E will not be equal to zero. In order to reduce E to zero, a relationship between E and the wall coordinates must be determined which can be employed to reduce E to zero. In previous works, Refs. 5 and 11, this relationship was determined numerically and required approximately 80% of the total computational time. However, the total running times were not excessive since the flowfields were isentropic, resulting in relatively rapid computations. However, for the current work and those involving more complex gas dynamic models, the basic computational times are measured in minutes, not seconds. Therefore, a technique that provides a simple relationship between the wall contour and the error function and eliminates as much numerical work as possible is required. Such a technique is presented below.

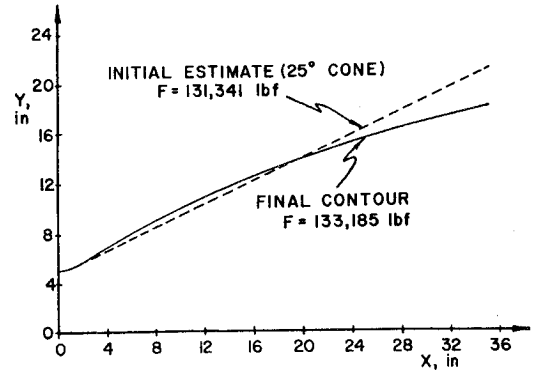

Fig. 3 Nozzle contours for convergence example.

It is seen that Eq. (44) explicitly contains $\dot{\eta}$. If it is assumed that the variables in Eq. (44) do not change appreciably with small changes in the nozzle contour, it appears reasonable to expect that solving Eq. (44) for $\dot{\eta}$ (for $E = 0$) would yield the optimum value, or at least a value closer to it than the original value of $\dot{\eta}$. Performing this iteration yields the following result for $\dot{\eta}$:

$$\dot{\eta} = \lambda_3/[\lambda_2 - (1 + d\delta/d\eta)(\eta + \delta)^p] \tag{45}$$

The new contour $\eta(x)$ is determined by integrating Eq. (45). Thus

$$\eta(x) = \eta(x_I) + \int_{x_I}^{x} \dot{\eta}(x)dx \tag{46}$$

This scheme is very simple and requires a negligible amount of numerical computation. Experience with this relaxation technique has shown that it converges rapidly and that convergence can be greatly enhanced by the judicious use of a variable weighting factor applied to the predicted changes of the wall slopes. To illustrate the behavior of the scheme, the following example case is presented.

The example selected was a constant length nozzle, 35-in.-long with a throat radius of 5 in. and an initial expansion section radius of curvature of 2.5 in. The gas thermodynamic properties, which were assumed to be constant, are: $\gamma = 1.2$, $R = 60$ (ft-lbf/lbm-°R), $P_0 = 1000$ psia, $T_0 = 5000$°R, and $\mu_0 = 5(10)^{-6}$ lbm/ft-sec. Sauer's transonic analysis[14] using an upstream throat radius of curvature of 15 in. was used to determine the start line. The boundary-layer model employed is discussed in Ref. 13. The nozzle exhausts to a 3 psia back pressure. The first estimate of the contour was a 25° cone, and is shown in Fig. 3, as is the final contour. The convergence criterion for all point values of the nondimensionalized error function was 0.0001, and ten iterations

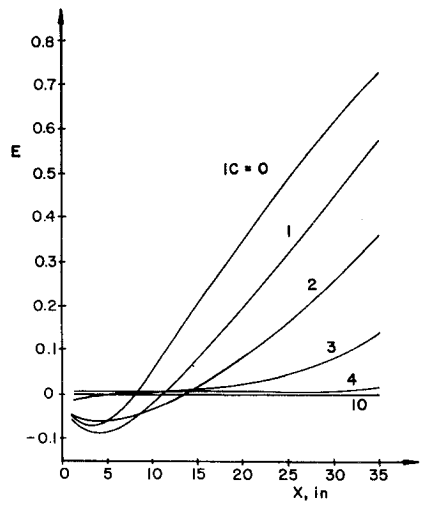

Fig. 4 Error function behavior for example.

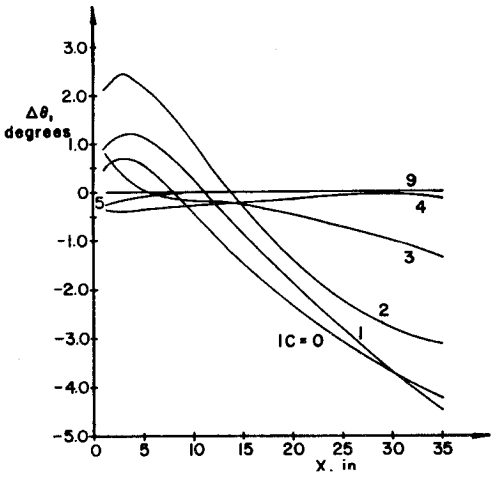

Fig. 5 Wall angle behavior for example.

of the wall were required to achieve this condition. The behavior of the error function is shown in Fig. 4 at various stages of the iteration process. $IC = 0$ designates values of the error function for the first estimate of the contour, $IC = 1$ after 1 iteration, etc. The absolute value of error function decreases after each successive iteration except for slight increases near the nozzle entrance after the first and second iterations. The rapid decrease on the third iteration is a result of the application of a variable weighting factor applied to the predicted wall slopes after the second iteration. The weighting factor varied linearly in x from 1.5 at point I to 0.7 at point F. The changes in the wall angle vary in a manner similar to the error function, but with opposite signs (see Fig. 5). Again, the sharp change in the calculated wall angle correction determined after the first and second iteration is a result of the employment of the variable weighting factor.

Although ten iterations were required to reduce all the point values of the error function to within the limits of the convergence criterion, the thrust approached the final value much sooner. After three iterations the thrust was 133,167 lbf, compared with 131,341 lbf for the first estimate. After four iterations, the thrust was 133,182 lbf, and the final value was 133,185 lbf. This result indicates the severity of the convergence criterion in regard to performance considerations, but as illustrated in Fig. 5, significant adjustments to the entrance portion of the contour continued to occur after the third iteration.

Parametric Study

Objectives

The purpose of this parametric study was to ascertain the order of magnitude of the performance increase that is possible by considering in the design process the actual nonequilibrium gas chemistry. Boundary-layer effects were not considered in the parametric study, since the performance improvement obtained by including these effects has been shown to be small (Hoffman, Scofield and Thompson[15]). No variations in the upstream geometry were considered. For flows which freeze near the throat, increasing the throat radius of curvature may increase performance substantially.

Table 1 General gas model, GGM, properties

Property	Molecule	Atom
Molecular weight, W	40.0	20.0
Specific heat, C_p, cal/mole-°K	9.0	5.0
Enthalpy, h_{ref}, kcal/mole	50.0	80.0
Entropy s_{ref}, cal/mole-°K	65.0	50.0

Table 2 Effect of reaction rate

Type of optimum contour	Nozzle thrust, lbf Type of flow chemistry: Equil. $kr = \infty$	Nonequil. $krT = 10^{19}$	Nonequil. $krT = 10^{18}$	Nonequil. $krT = 10^{17}$	Frozen $kr = 0$
Equil. $kr = \infty$	2400	2379	2334	2296	2284
Nonequil. $krT = 10^{19}$	2399	2385	2340	2300	2289
Nonequil. $krT = 10^{18}$	2393	2383	2343	2302	2290
Nonequil. $krT = 10^{17}$	2393	2382	2341	2302	2290
Frozen $kr = 0$	2393	2381	2340	2302	2290

Although this effect could be investigated parametrically, no such studies were conducted during this investigation.

Gas Chemistry Effects

The study of nonequilibrium gas chemistry effects was based on a reference gas chemistry model, termed the General Gas Model (GGM), for which the effects on thrust performance of changes in the reaction rate, nozzle size, stagnation temperature and molecular weight were evaluated. The gas model was chosen to be representative of the properties of the common diatomic gases. The GGM properties are listed in Table 1. The reference temperature T_{ref} at which h_{ref} and s_{ref} are evaluated is 4500°R. The nominal value of the reverse reaction rate k_r was chosen as $10^{18}T^{-1}$cm^6/mole^2-sec. The nozzle stagnation temperature and pressure were selected as 6320°R and 800 psia.

The geometrical constraint selected was a fixed length nozzle with a length of 7.0 in. The throat radius was 1 in., and the radius of curvature of the initial expansion contour was 0.5 in. The flow was assumed to be in equilibrium up to the supersonic initial-value line, which was chosen as a 10° source flow line with an equilibrium Mach number of 2. This start line was selected as representative of the conditions that might exist at the nozzle entrance of a scramjet type engine operating at an altitude of 50,000 to 100,000 ft at a flight Mach number of 10. The ambient pressure was set equal to zero.

In order to obtain the properties along the start line and the equilibrium and frozen flow properties in the expansion section, a table of the GGM flow properties was generated with a general thermochemistry program. The values of the velocity, pressure, density, temperature and atomic mass fraction at the start line were 5692.1 fps, 107.72 psia, 0.0704 lbm/ft^3, 5232°R, and 0.0901, respectively. The frozen Mach number was 1.866.

The object of Case 1 was to determine the effect of variations in the reaction rate, within the probable limits of uncertainty, on gross thrust and thrust improvement obtained by optimization of the nozzle contour. From Cherry,[11] the degree of uncertainty in the reaction rates of the common diatomic gases is a factor of $10^{\pm 1}$. Thus, five optimum nozzles were generated, one for each of the following flow chemistry models: equilibrium with $k_r = \infty$, nonequilibrium with $k_rT = 10^{19}$,10^{18}, and 10^{17}, and frozen with $k_r = 0$. These five optimum nozzles were then analyzed with each of the other four flow chemistry models. The resulting gross thrust data are presented in Table 2, and the nozzle contours are illustrated in Fig. 6. Optimum nozzles appear along the upper left to lower right diagonal of Table 2.

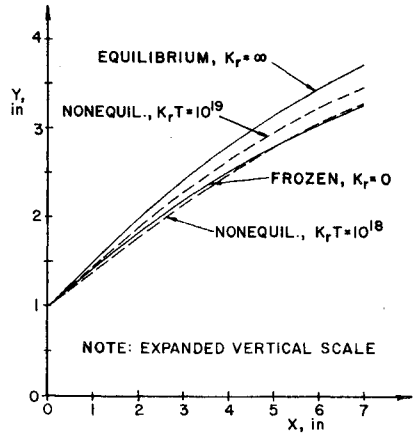

Fig. 6 Optimum contours for Case 1.

The thrust improvement obtained in the design process is obtained by comparing the thrust difference of the various nozzle-flow chemistry combinations. The maximum potential thrust improvement is the difference in the equilibrium and frozen values, and is 110 lbf, or approximately 5% of gross thrust for this case. If the actual flow were frozen, the thrust improvement obtained by designing for frozen flow would be 6 lbf over the optimum equilibrium nozzle analyzed with frozen flow. If the flow was actually in chemical equilibrium, then designing for equilibrium flow results in a thrust increase of 7 lbf over the optimum frozen contour analyzed with equilibrium flow. However, the flow through many propulsion nozzles is neither frozen nor in equilibrium but rather in a state of chemical nonequilibrium. Thus, if the value of the reverse reaction rate is $10^{18}T^{-1}$ and finite rate chemistry effects are considered in the design process, an actual nozzle thrust of 2343 lbf would be obtained. This represents a 9 lbf increase over the equilibrium nozzle design and a 3 lbf increase over the frozen nozzle design when each are analyzed with nonequilibrium flow.

Table 2 also presents the gross thrust data for the variation of k_r within the probable limits of uncertainty (i.e., for $k_rT = 10^{19}$ and 10^{17}). The variation of gross thrust as a function of the reaction rate is quite significant, varying up to within 15 lbf of the equilibrium value and down to within 12 lbf of the frozen value. However, the variation in thrust obtainable for each of the three reaction rate models considered varies by at most 3 lbf in each of the three nozzles designed for nonequilibrium flow. Thus, it would appear that the effect of variations in the reaction rate within the probable

Table 3 Effect of nozzle scaling

Type of optimum contour	Nozzle thrust, lbf Type of flow chemistry: Equil. $k_r = \infty$	Nonequil. $k_rT = 10^{18}$	Frozen $k_r = 0$
Equil. $k_r = \infty$	(21602) 21602	(21005) 21217	(20554) 20553
Nonequil. $k_rT = 10^{18}$	(21537) 21561	(21083) 21273	(20608) 20605
Frozen $k_r = 0$	(21533) 21534	(21063) 21259	(20611) 20611

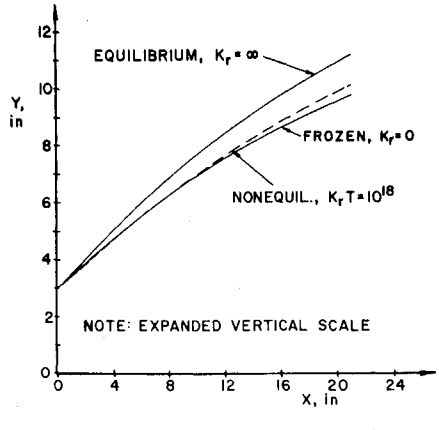

Fig. 7 Optimum contours for Case 2.

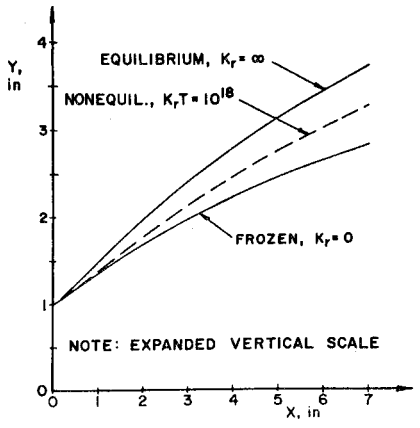

Fig. 8 Optimum contours for Case 3.

limits of uncertainty is not as critical a factor on the nozzle design as is the inclusion of the finite rate effects themselves.

Figure 6 illustrates the contours of the equilibrium, nonequilibrium with $k_rT = 10^{19}$ and 10^{18}, and frozen optimum nozzles. There is a decided difference between the contours, with the nonequilibrium contours being closer to the frozen contour than to the equilibrium contour. Although the performance of all the nonequilibrium nozzles is between the limits of the equilibrium and frozen nozzles, this is not the case for the shapes of all the optimum contours. The equilibrium and frozen nozzles both open up more rapidly than does the nonequilibrium nozzle with $k_rT = 10^{18}$. This result is expected since equilibrium and frozen flows can expand rapidly (with no process loss occurring), and once sufficiently expanded, the flow can be rapidly turned back toward the axial direction to reduce the divergence loss. However, the nonequilibrium flow process has an extra degree of freedom, the degree of recombination, which governs the amount of thermal energy released. As a result, the finite-rate nozzle contours do not, in general, expand as rapidly as do the isentropic nozzles in order to avoid freezing the flow. This permits the release of additional thermal energy which can then be converted into directed kinetic energy.

Case 2 investigated the effect of nozzle size on the relative performance and shape of the optimum nozzle. The geometry of the reference nozzle was scaled up by a factor of three, thus increasing the mass flow rate by a factor of 9. The resulting nozzle has a length of 21 in., a throat radius of 3 in. and an initial expansion section radius of curvature of 1.5 in. The performance values are presented in Table 3, and the optimum contours are illustrated in Fig. 7. The numbers in parentheses above the thrust values in Table 3 are the scaled values obtained by multiplying the results of Case 1 by 9. Again, optimum contours appear along the diagonal. All values scale exactly by 9 except the nonequilibrium performance values, and the thrust of all three contours analyzed with nonequilibrium flow has shifted upward toward the equilibrium value. This is as expected, since the flow stay time in the nozzle, and thus the amount of recombination, is greater for the larger nozzle. The thrust improvement obtained by considering the finite rate chemistry effects in the design process has also changed. The values are 56 lbf when compared with the optimum equilibrium contour analyzed with nonequilibrium flow, and 14 lbf when compared to the optimum frozen contour analyzed with nonequilibrium flow. The maximum potential recovery for this case is 991 lbf. This result would tend to indicate that the percentage of the maximum potential thrust recovery which can actually be recovered by considering nonequilibrium effects in the design process decreases with increasing nozzle size. As illustrated in Fig. 7, the shape of the optimum nonequilibrium nozzle does not scale with the size of the nozzle. This is seen by noting that the cross point of the nonequilibrium and frozen contours occurs approximately six inches downstream of the throat for both the 7-in.- and 21-in.-long nozzles.

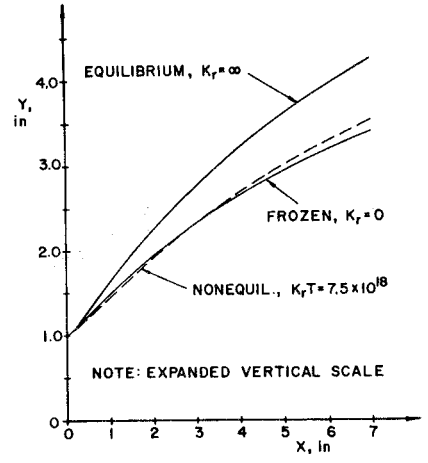

Fig. 9 Optimum contours for Case 5.

Table 4 Effect of stagnation temperature

Type of optimum contour	Nozzle thrust, lbf Type of flow chemistry		
	Equil. $k_r = \infty$	Nonequil. $k_rT = 10^{18}$	Frozen $k_r = 0$
Equil. $k_r = \infty$	2494	2459	2267
Nonequil. $k_rT = 10^{18}$	2489	2473	2285
Frozen $k_r = 0$	2461	2460	2294

In Case 3, the effects of stagnation temperature were investigated. The stagnation temperature was raised to 9065°R and lowered to 3600°R. At the lower temperature there was effectively no difference between the equilibrium and frozen performance or contours. The thrust of both nozzles was the same to five significant figures (2430.0 lbf). However, for the higher temperature, chemistry effects were significant. The atomic mass fraction at the start line increased to 0.712 from 0.090 for Case 1. The start line properties p, T, ρ, and V for an equilibrium Mach number of 2 were: 110 psia, 7002°R, 0.0342 lbm/ft^3, and 8381 fps, respectively. Again, equilibrium, nonequilibrium with $k_rT = 10^{18}$, and frozen optimum contours were generated. The performance values are presented in Table 4, and the contours are illustrated in Fig. 8. Using the nominal value of the reaction rate results in a flow that is much closer to equilibrium, the optimum nonequilibrium thrust being only 21 lbf less than the optimum equilibrium thrust, whereas the difference between the optimum frozen and equilibrium thrusts has increased almost 100% to 200 lbf. The thrust improvement of the optimum equilibrium nozzle over the frozen contour analyzed with equilibrium chemistry has

Table 5 Effect of molecular weight

Type of optimum contour	Nozzle thrust, lbf Type of flow chemistry		
	Equil. $k_r = \infty$	Nonequil. $k_rT = 10^{18}$	Frozen $k_r = 0$
Equil. $k_r = \infty$	2400	2326	2284
Nonequil. $k_rT = 10^{18}$	2393	2335	2290
Frozen $k_r = 0$	2393	2333	2290

Table 6 Hydrogen gas model properties

Property	Molecule	Atom
Molecular weight, W	2.016	1.008
Specific heat, C_p, cal/mole-°K	8.266	4.968
Enthalpy, h_{ref}, kcal/mole	14.672	54.656
Entropy, s_{ref}, cal/mole-°K	45.004	36.848

also increased to 33 lbf, and an increase in the thrust of 27 lbf was obtained for the optimum frozen nozzle over the equilibrium contour analyzed with the frozen flow. The increases in the thrust of the optimum nonequilibrium nozzle over the equilibrium and frozen contours analyzed with nonequilibrium flow were 14 lbf and 13 lbf, respectively. Thus, all the thrust improvements, except for the optimum nonequilibrium nozzle over the equilibrium contour analyzed with nonequilibrium flow, have increased over the values obtained in Case 1. This is as expected, since there has been a shift of the nonequilibrium performance toward the equilibrium performance, thereby decreasing the difference between them and the amount of thrust that can potentially be recovered.

The effects of molecular weight were studied in Case 4. For this case, the per mole properties of the GGM were held constant and the molecular weights halved. The only change from Case 1 that occurred in thrust or in the nozzle contour was associated with the nonequilibrium flow model, and was due to a reduction of the effective reaction rate. This result is illustrated in Table 5 by the reduction of the thrust to 2335 lbf from 2343 lbf for Case 1. These results also show that the thrust for the equilibrium and frozen flow optimum nozzles remains constant at the values for Case 1, even though the molecular weight has decreased.

Up to this point, only the artificial gas model developed for this parametric study has been considered in the performance comparisons. In order to substantiate these values as being representative of the effects and improvements of a real propellant system, an analysis was performed for the hydrogen gas system in Case 5. A nozzle of the same geometry and size as considered in Case 1 was used. The properties of the gas are presented in Table 6. The reference temperature T_{ref} was 3600°R and the nominal value of the reverse reaction rate, taken from Cherry,[16] was $k_r = 7.5(10)^{18}T^{-1}cm^6/mole^2$-sec. An equilibrium and frozen flow property table was generated, and an equilibrium, ten degree source flow start line was established with a velocity of 16,445 fps and equilibrium and frozen Mach numbers of 1.1545 and 1.060, respectively. The nozzle inlet stagnation temperature and pressure were 6350°R and 175 psia, respectively. These conditions were chosen to be representative of the conditions that might eventually be expected to exist in a high performance nuclear rocket engine. Equilibrium, nonequilibrium, and frozen optimum nozzles were then generated and cross analyzed with the 3 different flow chemistries. The thrust of each nozzle-chemistry combination is presented in Table 7, and the nozzle contours are illustrated in Fig. 9. There is a 97.2 lbf difference in the performance of the equilibrium and frozen optimum nozzles, and the performance of the optimum finite rate nozzle is about midway between the equilibrium and frozen nozzle performances. This was also the case for Case 1. The thrust improvements of the optimum equilibrium nozzle over the optimum frozen contour analyzed with equilibrium flow and vice versa were 9.5 lbf and 7.8 lbf, respectively. The thrust improvements of the optimum nonequilibrium nozzle over the equilibrium and frozen contours analyzed with nonequilibrium flow were 8.9 lbf and 1.7 lbf, respectively. As illustrated in Fig. 9, there is also a marked difference between the frozen and equilibrium contours, as in Case 1. The optimum nonequilibrium contour is again closer to the frozen than to the equilibrium contour and has a more gradual expansion in order to avoid freezing the flow.

Table 7 Hydrogen gas performance comparison

Type of optimum contour	Nozzle thrust, lbf Type of flow chemistry: Equil. $k_r = \infty$	Nonequil. $k_rT = 7.5\ 10^{18}$	Frozen $k_r = 0$
Equil. $k_r = \infty$	971.4	917.5	866.4
Nonequil. $k_rT = 7.5\ 10^{18}$	964.1	926.4	873.9
Frozen $k_r = 0$	961.9	924.7	874.2

Conclusions

A formulation of the maximum thrust nozzle problem was presented which includes the effects of finite rate chemical reactions for the flow of a simple dissociating gas, variations in stagnation conditions across the flowfield (rotational flow) for a frozen or equilibrium gas mixture, and the losses associated with the boundary layer. A parametric study was conducted to determine the magnitude of the performance increases which may be obtained by accounting for nonequilibrium chemical reactions in the design process. The results indicate that significant increases in nozzle performance may be obtained when the actual nonequilibrium flow chemistry is employed in the design process. In most cases, the optimum nonequilibrium nozzle contour was close to the optimum frozen nozzle contour. This suggests that, when designing nozzles for nonequilibrium flows, frozen flow designs approach the actual nonequilibrium design more closely than do equilibrium designs, and should be employed if actual nonequilibrium designs such as presented herein are not performed.

References

[1] Guderley, G. and Hantsch, E., "Beste Formen für Achsensymmetrische Überschallschubdüsen," *Zeitschrift für Flugwissenschaften*, Vol. 3, No. 9, Sept. 1965, pp. 305–313.

[2] Rao, G. V. R., "Exhaust Nozzle Contour for Optimum Thrust," *Jet Propulsion*, Vol. 28, No. 6, June 1958, pp. 377–382.

[3] Guderley, G., "On Rao's Method for the Computation of Exhaust Nozzles," *Zeitschrift für Flugwissenschaften*, Vol. 7, No. 12, Dec. 1959, pp. 345–350.

[4] Guderley, K. G. and Armitage, J. V., "General Approach to Optimum Rocket Nozzles," *Theory of Optimum Aerodynamic Shapes*, edited by A. Miele, Academic Press, New York, 1965, Chap. 11, pp. 161–183.

[5] Appleton, J. P., "On the Maintenance of Chemical Equilibrium during the Expansion of Reacting Gas Mixtures, the Optimum Nozzle Design," A.A.S.U. Rept. 216, March 1962, Univ. of Southampton, Hampshire, England.

[6] Burwell, W. G., Sarli, V. J., and Zupnik, T. F., "Analytically Determined Nonequilibrium Mixture Properties in High Expansion Ratio Nozzles," Paper presented at the Third Conference on the Performance of High Temperature Systems, Pasadena, Calif., Dec. 7–9, 1964.

[7] Kraiko, A. N., "Variational Problems of Gas Dynamics of Nonequilibrium and Equilibrium Flows," *Prikladnaia Matematika i Mekhanika*, Vol. 28, No. 2, Feb. 1964, pp. 285–295.

[8] Kraiko, A. N., Naumova, I. N., and Shmyglevskii, Iu. D., "On the Construction of Bodies of Optimum Shape in a Supersonic Stream," *Prikladnaia Matematika i Mekhanika*, Vol. 28, No. 1, Jan. 1964, pp. 178–181.

[9] Galyun, N. S. and Kraiko, A. N., "A Variational Problem in One-Dimensional Nonequilibrium Gas Dynamics," *Izvestiya, Mekhanika Zhidkosti i Gaza*, No. 2, 1966, pp. 27–36.

[10] Hoffman, Joe D., "A General Method for Determining Optimum Thrust Nozzle Contours for Chemically Reacting Gas Flows," *Journal of the American Institute of Aeronautics and Astronautics*, Vol. 5, No. 4, April 1967, pp. 670–676.

[11] Scofield, M. Peter, Thompson, H. Doyle, and Hoffman,

Joe D., "Thrust Nozzle Optimization Including Boundary Layer Effects," AFAPL-TR-67-158, Dec. 1967, Air Force Aero Propulsion Lab., Wright-Patterson Air Force Base, Ohio.

[12] Hoffman, Joe D., Scofield, M. Peter, and Thompson, H. Doyle, "Thrust Nozzle Optimization for Nonequilibrium, Chemically Reacting Flows Including Boundary Layer Effects," AFAPL-TR-69-49, April 1969, Air Force Aero Propulsion Lab., Wright-Patterson Air Force Base, Ohio.

[13] Scofield, M. Peter and Hoffman, Joe D., "Maximum Thrust Nozzles for Rotational and Nonequilibrium Simple Dissociating Gas Flows Including Boundary Layer Effects," AFAPL-TR-69-85, Oct. 1969, Air Force Aero Propulsion Lab., Wright-Patterson Air Force Base, Ohio.

[14] Sauer, R., "General Characteristics of the Flow through Nozzles at Near Critical Speeds," TM 1147, June 1947, NACA.

[15] Hoffman, Joe D., Scofield, M. Peter, and Thompson, H. Doyle, "Thrust Nozzle Optimization Including Boundary Layer Effects," *The Journal of Optimization Theory and Applications*, to be published.

[16] Cherry, S. S., "Phase II Final Report, Screening of Reaction Rates," Rept. 08832-6002-T000, Dec. 1967, TRW Systems Group, Redondo Beach, Calif.

SEPTEMBER 1971 AIAA JOURNAL VOL. 9, NO. 9

Reactive Stream Separation Photography

D. T. Campbell,* S. D. Clapp,† R. L. Proffit,‡ and G. L. Cline§
Rocketdyne, A Division of North American Rockwell Corporation, Canoga Park, Calif.

High-speed photographic techniques were used to study impinging streams of nitrogen tetroxide and hydrazine in an experimental investigation of reactive stream separation. The high-resolution color motion pictures obtained show the detailed behavior of the liquid streams, spray fan, and individual droplets within the combustion zone. For the first time, reactive stream separation was shown to result from a cyclic phenomenon in which the streams meet, form a spray fan, are literally blown apart by a detonation or explosive deflagration, and then reform. Blowapart frequencies and magnitudes were correlated with jet diameters and injection velocities.

Introduction

DIRECT impingement of liquid streams can be used as an efficient means of mixing two liquids as well as atomizing them. This technique has found frequent application with liquid rocket engines. As first reported (1959) by Elverum and Staudhammer,[1] however, impinging hypergolic liquid streams may, under certain conditions and probably as a result of their chemical reactivity, tend to separate or be blown apart rather than achieving the intended degree of mixing.

Continued experimental investigation by Johnson, Riebling, et al.,[2-7] of impinging jets or sheets of nitrogen tetroxide and hydrazine in baffled or divided chambers, confirmed Elverum's photographic indication of fuel/oxidizer stratification. By auxiliary injection of fuel and oxidizer downstream of the chamber divider, performance changes could be used to monitor the presence of unmixed propellants from the main injection element. This work showed that the incidence of separation was dependent upon orifice sizes, becoming more pronounced as the orifice size was increased.

Since 1966, interest in blowapart or reactive stream separation, as it has alternately been called, was evidenced by both in-house and contractual work by NASA-JPL, NASA-LeRC, and by the Air Force (AFRPL). Most of the experimental methods have involved photography[8-12] in which color stratification in the combustion zone downstream of the propellant impingment location was interpreted to signify blowapart.

Kushida and Houseman[13] made a first attempt to develop an analytical model to predict when separation would or would not occur. This model included two regimes, depending upon the pressure of the environment. At low-to-moderate pressures, separation was presumed to result from liquid/liquid interfacial reaction and was thus dependent upon a residence time as indexed by the jet diameter divided by the injection velocity (D/V) and upon the propellant injection temperature. At some higher pressure, the value of which depended upon D/V, a gas phase reaction was presumed to sustain the liquid stream separation. Lawver, Breen, et al.[8] obtained still photographic data which seemed to verify the significance of D/V and propellant temperature. Their semiempirical model, developed somewhat differently from that of Kushida, emphasized the strong effect of liquid temperatures through an Arrhenius reaction rate expression. Unfortunately, however, as reported by Zung,[9] much of the Ref. 8 data are now considered questionable due to oxidizer boiling as it was injected and to propellant reaction with lucite windows of the experimental apparatus.

In summary, by the summer of 1969, blowapart was widely recognized as a phenomenon that should be characterized for the injector designer. However, design and operating conditions conducive to separation had not been adequately delineated, even for the much-studied nitrogen tetroxide/hydrazine system. Data for nitrogen tetroxide with other hydrazine-type fuels were sparse. No photographic techniques had yet been demonstrated that could provide uncontroversial data as to when separation did or did not occur. The physical nature of the separation process, when it did occur, was generally presumed to involve a quasi-steady lamination of the spray fans with fuel on one side and oxidizer on the other.

This paper provides the results of an experimental photographic study which for the first time dramatically describes

Presented as Paper 70-608 at the AIAA 6th Propulsion Joint Specialist Conference, San Diego, Calif., June 15–19, 1970; submitted July 14, 1970; revision received November 30, 1970. The work reported herein was performed under NASA-JPL sponsorship under Contract NAS7-720. The authors would like to express their appreciation to the NASA-JPL contract technical managers, J. Rupe and M. Caylton, and to J. Cordill, E. Rojec, T. Sloat, and S. Zeldin, who aided in the collection and evaluation of the experimental data.

* Manager, Propulsion Technology. Member AIAA.
† Program Manager, Advanced Propulsion Technology. Member AIAA.
‡ Member of the Technical Staff.
§ Member of the Technical Staff.